Journal of Natural Gas Science and Engineering 25 (2015) 236–241

Contents lists available at ScienceDirect

Journal of Natural Gas Science and Engineering

journal homepage: www.elsevier.com/locate/jngse

Effects of changes in pipe cross-section on the explosion-proof distance and the propagation characteristics of gas explosions

Liutao Sun [a, b], Bingyou Jiang [a, c, *], Fanjun Gu [b]

[a] State Key Laboratory of Coal Resources and Safe Mining, China University of Mining and Technology, China
[b] School of Safety Engineering, China University of Mining and Technology, China
[c] School of Mining and Safety Engineering, Anhui University of Science & Technology, China

ARTICLE INFO

Article history:
Received 25 December 2014
Received in revised form
4 May 2015
Accepted 6 May 2015
Available online 15 May 2015

Keywords:
Pipe cross-section
Gas explosion
Explosion-proof safety distance
Flame-proof distance

ABSTRACT

After establishing a pipe model with a length of 100 m, the propagation characteristics of gas deflagrations were simulated using AutoReaGas software for pipe cross-sectional areas of 0.04 m × 0.04 m, 0.08 m × 0.08 m, 0.12 m × 0.12 m and 0.16 m × 0.16 m. The results showed that the pipe cross-section had a distinct effect on the overpressure, density, temperature, gas velocity and combustion rate of gas explosions. Specifically, as the equivalent pipe diameter increased, the maximum overpressure, density, temperature, gas velocity and combustion rate at each gauge point decreased. As the equivalent pipe diameter increased, the flame arrival time at each gauge point was consequently delayed. In addition, the increase in the equivalent pipe diameter decreased the explosion-proof distance, as well as the dimensionless safety distance. In addition, increasing the equivalent pipe diameter can largely reduce the dimensionless flame-proof distance, thereby making mining workers immune to the threat of gas explosion shockwaves.

1. Introduction

Recently, as coal exploitation has extended to increasing depths, the number of gas outbursts has increased drastically and excessive gas stimulation has occurred at times. When combined with the incidence of sparks produced by the friction of coal cutters, tunnel boring machines, conveyor belts, etc., gas explosions have become more likely to occur. After analyzing 563 gas explosion cases in China that occurred from 1988 to 2008, Li et al. (2010) concluded that 232 accidents occurred at mining working faces, accounting for 41.2% of all cases, and that 159 cases, accounting for 28.2% of all cases, occurred at heading faces, with the remaining 117 cases, accounting for 20.8% of all cases, occurring separately at haul roads, crossheadings, etc. Thus, it is clear that working faces are quite prone to gas explosions. We therefore explored the propagation characteristics of gas explosions, thereby calculating the explosion-proof distance and providing guidance for gas explosion prevention.

When a gas explosion shockwave propagates through a tunnel, the consumption of the gas is accompanied by irreversible energy losses, such as by heat conduction and thermal radiation; thus, during wave propagation, the power of the shockwave decays and finally transforms into a sound wave (Wang and Xie, 1989). A minimum crow-fly distance, i.e., the explosion-proof distance, can therefore be calculated. The explosion-proof distance can be defined as the distance from the explosion source to the location where the shock wave attenuates to a sound wave along a straight roadway. Gas explosion shockwaves can not only demolish facilities in tunnels but also trigger dust explosions. Wang et al. (2012) studied the effect of tunnel cross-section on shockwave propagation and established a relationship between shockwave decay and tunnel cross-section. Using finite element software, Lu and Liu (2009) simulated the shockwave attenuation law in tunnels of different section shapes. Jia et al. (2007) established a mathematical model based on the propagation law of a shockwave with a sudden change in cross-section. Additionally, some researchers have studied the propagation characteristics of shockwaves in crooked tunnels (Jia et al., 2011; Wang and Li, 2004). In addition, the flame acceleration mechanism and the process by which a shockwave transforms into a detonation have been widely researched (Blanchard et al., 2011; Chan and Dewit, 1996; Dorofeev, 2011; Grune et al., 2013; Oran and Gamezo, 2007; Silvestrini et al., 2008; Thomas et al., 2010). Nevertheless, although the study of explosion distance is widespread in many fields, such as

* Corresponding author. School of Mining and Safety Engineering, Anhui University of Science & Technology, Huainan, Anhui 232001, China.
E-mail address: cumtjiangby@163.com (B. Jiang).

http://dx.doi.org/10.1016/j.jngse.2015.05.007
1875-5100/

engineering blasting, liquefied natural gas explosion and fire prevention (Feng, 2007; Wang, 1982; Xia et al., 2012), little research is focused on its application in the coal mining industry. Jiang et al. (2012a, 2014) emphasized the effect of the initial temperature on the explosion-proof distance and calculated the gas explosion-proof distance using numerical simulation. In this paper, utilizing a numerical analysis tool, AutoReaGas, we sought to reveal the law of gas explosion propagation and calculate the explosion-proof distance.

2. Gas explosion model

In a mathematical model simulation, the gas explosion process can be treated as the thermal expansion process of an ideal gas, and the gas dynamics process can be captured by the equations of mass conservation, momentum conservation, energy conservation and fuel components within a Cartesian coordinate system as follows (Jiang et al., 2012b):

Continuity equation:

$$\frac{\partial \rho}{\partial t}+\frac{\partial}{\partial x_j}(\rho u_j)=0 \tag{1}$$

Momentum conservation equation:

$$\frac{\partial}{\partial t}(\rho u_i)+\frac{\partial}{\partial x_j}(\rho u_j u_i)=-\frac{\partial p}{\partial x_i}+\frac{\partial \tau_{ij}}{\partial x_j} \tag{2}$$

Energy conservation equation:

$$\frac{\partial}{\partial t}(\rho E)+\frac{\partial}{\partial x_j}(\rho u_j E)=\frac{\partial}{\partial x_j}\left(\Gamma_E\frac{\partial E}{\partial x_j}\right)-\frac{\partial}{\partial x_j}(p u_j)+\tau_{ij}\frac{\partial u_i}{\partial x_j} \tag{3}$$

Fuel component equation:

$$\frac{\partial}{\partial t}\left(\rho m_{fu}\right)+\frac{\partial}{\partial x_j}\left(\rho u_j m_{fu}\right)=\frac{\partial}{\partial x_j}\left(\Gamma_{fu}\frac{\partial m_{fu}}{\partial x_j}\right)+R_{fu} \tag{4}$$

Turbulence is an important factor in explosive gas combustion; using the k–ε turbulence model, the turbulent kinetic energy k equation (Ciccarelli and Dorofeev, 2008) is as follows:

$$\frac{\partial}{\partial t}(\rho k)+\frac{\partial}{\partial x_j}(\rho u_j k)=\frac{\partial}{\partial x_j}\left(\Gamma_k\frac{\partial k}{\partial x_j}\right)+\tau_{ij}\frac{\partial u_i}{\partial x_j}-\rho\varepsilon \tag{5}$$

The equation of the turbulent kinetic energy dissipation rate, ε, is as follows (Launder and Spalding, 1972):

$$\frac{\partial}{\partial t}(\rho\varepsilon)+\frac{\partial}{\partial x_j}(\rho u_j\varepsilon)=\frac{\partial}{\partial x_j}\left(\Gamma_\varepsilon\frac{\partial \varepsilon}{\partial x_j}\right)+C_1\frac{\varepsilon}{k}\tau_{ij}\frac{\partial u_i}{\partial x_j}-C_2\frac{\rho\varepsilon^2}{k} \tag{6}$$

$$\tau_{ij}=\mu_t\left(\frac{\partial u_i}{\partial x_j}+\frac{\partial u_j}{\partial x_i}\right)-\frac{2}{3}\delta_{ij}\left(\rho k+\mu_t\frac{\partial u_j}{\partial x_j}\right) \tag{7}$$

where ρ is the density; u_i is the particle velocity along coordinate direction i; p is the static pressure; $E=C_vT+m_{fu}H_c$ is the specific energy; k is the turbulent kinetic energy; m_{fu} is the fuel mass fraction; $\mu_t=C_\mu\rho k^2/\varepsilon$ is the turbulent viscosity; R_{fu} is the rate of volume combustion; C_v is the constant-volume specific heat; T is the temperature; H_c is the combustion heat; Γ is the turbulent dissipation coefficient of transport properties; δ_{ij} is the Kronecker operator; i and j are the coordinate directions; and C_1, C_2 and C_μ are the turbulence model constants.

The turbulence intensity u' and the feature size of turbulence L_t are given as follows (Favre, 1969):

Table 1
Relative error between two different grid cell sizes at various distances.

Position (m)	Experimental results (MPa)	Numerical results (MPa) and relative error			
		4 × 4 × 1000		2 × 2 × 500	
0.5	1.0809	1.12317	3.91%	1.01	−6.56%
2.5	0.99738	0.92947	−6.81%	0.88	−11.77%
4.5	1.1128	1.14154	2.58%	1.04	−6.54%

$$u'=\sqrt{\frac{2}{3}k}\quad L_t=C_\mu^{0.75}\frac{k^{3/2}}{\varepsilon} \tag{8}$$

The relationship between the turbulence burning velocity, the turbulence parameters and the characteristics of the mixture parameters is (Bray, 1990)

$$S_t=1.8u'^{0.412}L_t^{0.196}S_l^{0.784}\nu^{-0.196} \tag{9}$$

where S_t is the turbulence burning velocity, m/s; S_l is the laminar burning velocity, m/s; and ν is the kinematic viscosity of the mixture, m^2/s.

3. Validation of the numerical method

To validate the numerical results with experimental data, an experimental apparatus was constructed, and numerical calculations simulating the experimental conditions were conducted.

The length and cross-sectional area of the experimental pipe were 5.0 m and 0.08 m × 0.08 m, respectively, and the two ends of the pipe were closed. The volumetric concentration of methane in the methane/air mixture was approximately 10%. Nine pressure sensors were placed along the pipe at 0.5-m intervals. Ignition was actuated at a closed end with a 2-J combustion engine spark plug. According to the experimental conditions, the methane/air explosion and its blast process were simulated using AutoReaGas.

The numerical simulation was performed using two different grid sizes to verify the sensitivity of the results to changes therein. One grid size was based on a 2 cm × 2 cm × 2 cm cubic cell, and the other was based on a 4 cm × 4 cm × 4 cm version, i.e., the numbers of cells were 16,000 and 2,000, respectively. The relative discrepancy between the two different grid cell sizes at various distances is presented in Table 1. As shown in the table, the 2 cm × 2 cm × 2 cm cube cell grid was observed to be more accurate. The relative error between the calculated and the experimental results may have

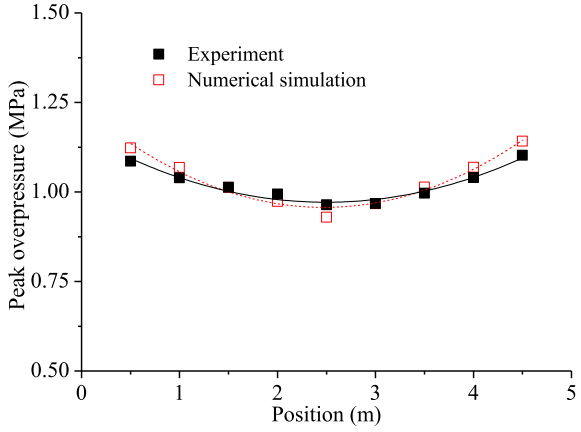

Fig. 1. Comparison between the AutoReaGas software model and the experimental results.